Interference Fading Mitigation in Coherent Φ-OTDR Based on Subband Phase-Shift Transform

Yafeng Cheng, Hanyong Wang, Desheng Li, Ying Qiu, Ming Luo, Xu Zhang, Jing Zhang, Zhichao Wu, Tianye Huang, *Member, IEEE*, and Xiang Li, *Associate Member, IEEE*

***Abstract*—In this paper, an interference fading mitigation method based on subband phase-shift transform in coherent phase-sensitive optical time-domain reflectometer (Φ-OTDR) is proposed. The operation principle of the subband phase-shift transform with complementary amplitude characteristic is presented. The phase shift transform is performed in the digital domain without requiring complex frequency modulation. After subband phase-shift transform, the interference fading can be effectively mitigated through optimal tracking and rotated vector sum (RVS) methods. The experimental results show that the fluctuation of phase intensity is reduced from ∼70 dB to ∼20 dB and the average standard deviation of the recovered phase is also reduced from 0.223 rad to 0.046 rad. In addition, different disturbance signals are successfully recovered, verifying the effectiveness of the proposed method.**

***Index Terms*—Distributed optical fiber sensor, interference fading, optical time domain reflectometry.**

I. Introduction

COMPARED with electrical sensors, distributed optical fiber sensor (DOFS) can provide continuous, real-time monitoring over long distances [1], [2], [3], which offers unparalleled advantages in terms of immunity to electromagnetic interference, easier installation and flexibility, multiplexing capability and wide measurement range. Among the DOFS technologies, phase-sensitive optical time domain reflectometry (Φ-OTDR) has received much attentions in the past decades due to its additional advantages including higher sensitivity, improved resolution in localization, and strong disturbance signal characterization ability. Conventional OTDR can measure the intensity of Rayleigh backscattered (RBS) light to identify the location of the events. However, conventional OTDR can only detect the inherent amplitude change information, and cannot detect the dynamic change. This is mainly because conventional OTDR uses large linewidth laser, which cannot accurately measure the small changes along the optical fiber. For Φ-OTDR, the Φ-OTDR can be roughly divided into intensity demodulation and phase demodulation categories. For intensity detection, it only identifies the disturbance location. The disturbance signal cannot be quantified accurately, because the signal strength is nonlinear to the external disturbance. It is noted that the phase change of the RBS light is linear to the external disturbance. Therefore, phase demodulation technology can accurately measure the external physical quantity changes, showing significant performance advantages and application potential. As far as we know, Φ-OTDR has been successfully used in the areas of geological structure exploration [4], structural health monitoring and pipeline detection [5], security surveillance [6], environmental monitoring and railway transportation monitoring [7], [8].

In Φ-OTDR, a coherent light source is used to generate a probe signal that is launched into the fiber. As the probe signal propagates along the fiber, it interacts with the fiber's mechanical disturbances, temperature changes, and strain. These interactions cause phase changes in the RBS light. In previous approaches, perturbations were usually extracted using intensity monitoring on RBS light. However, the relationship between the intensity of the disturbance event and signal is nonlinear [9]. Therefore, the disturbance event can only be located but not accurately quantified. In order to solve this issue, coherent Φ-OTDR is proposed to use phase detection and demodulation to accurately restore the disturbance signal [10], [11], [12], [13], [14]. In coherent Φ-OTDR, the RBS light overlaps each other at different positions, and the interference will occur among these RBS lights, resulting in amplitude fluctuations of the received electrical signal after photoelectric detection. If the amplitude of the electrical signal is too small, the phase cannot be accurately demodulated. This phenomenon is called the interference fading. Due to the existence of interference fading, large phase fluctuations still occur at the fading point, even if there is no external disturbance. This could be mistakenly identified by the system as a vibration caused by the external environment, resulting in a false alarm.

In order to eliminate the interference fading, an inner-pulse frequency-division method and the rotated-vector-sum (RVS) method was proposed in 2017, which can effectively overcome the interference fading without sacrificing the vibration frequency response and measurement range [15]. Following this idea, a spectrum extraction and remixing method (SERM) has also been proposed to mitigate the interference fading [16].

Manuscript received 9 August 2023; revised 4 September 2023; accepted 12 September 2023. Date of publication 18 September 2023; date of current version 27 September 2023. This work was supported by the Science and Technology Key Project of Wuhan under Grant 2023010302020030. *(Corresponding authors: Xiang Li; Tianye Huang.)*

Yafeng Cheng, Hanyong Wang, Desheng Li, Jing Zhang, Zhichao Wu, Tianye Huang, and Xiang Li are with the School of Mechanical Engineering and Electronic Information, China University of Geosciences, Wuhan 430074, China (e-mail: chengyf@cug.edu.cn; hanyong@cug.edu.cn; 20171002625@cug.edu.cn; zhangjing28@cug.edu.cn; wuzhichao@cug.edu.cn; tianye_huang@163.com; lix@cug.edu.cn).

Ying Qiu, Ming Luo, and Xu Zhang are with the State Key Laboratory of Optical Communication Technologies and Networks, China Information and Communication Technologies Group Corporation (CICT), Wuhan 430074, China (e-mail: yqiu@wri.com.cn; mluo@wri.com.cn; xzhang@wri.com.cn).

Digital Object Identifier 10.1109/JPHOT.2023.3316350

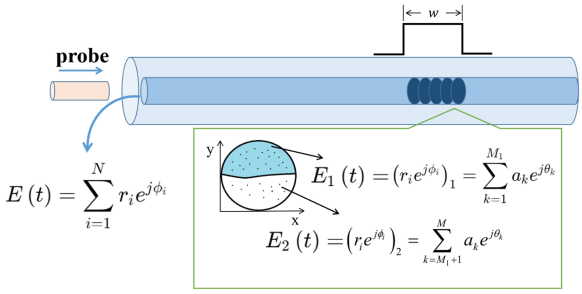

Fig. 1. Illustration of 2-D backscattering model of fiber.

This method eliminates most of the interference fading without requiring complex frequency modulation. Moreover, a spectrum extraction and the rotated-vector-sum (SERVS) method with a pulse-intensity-coding Φ-OTDR scheme has been proposed [17]. A multi-frequency Φ-OTDR scheme based on three acoustic optic modulators are also proposed to mitigate the interference fading with optimal tracking algorithm [18]. The proposed method can successfully predict the occurrences of the distortion in the output phase signal and avoid the distortion by selecting a phase signal with higher signal-to-noise ratio (SNR). A method utilizing negative frequency band in Φ-OTDR has also been proposed, aiming to double the available system bandwidth [19]. This method overcomes the inherent trade-off between sensing distance and scan-rate. A combination of positive and negative frequency multiplexing is employed in conjunction with frequency division multiplexing. Recently, an effective interference fading suppression method based on phase shift transform has been proposed [20]. This method effectively eliminates the interference fading after extracting and combining the subbands with different bandwidth multiple times followed by the RVS method.

In this work, we propose a method to mitigate the interference fading in coherent Φ-OTDR using subband phase-shift transform. By dividing the main lobe and the first-order sidelobes equally, and performing phase-shift with equal interval in the digital domain, only one-time transform is required with reduced computational complexity. Compared with the previous approach [20], it is demonstrated that fewer transform times can also achieve the effect of eliminating interference fading. The experimental results show that the fluctuation of the RBS light intensity can be reduced from ∼60 dB to ∼20 dB and the average standard deviation of differential phase is reduced from 0.223 rad to 0.046 rad. In addition, the vibrations of different waveforms are imposed onto the fiber under test, and the waveforms can be well recovered, which verifies the reliability of the proposed method.

II. Operation Principle

A. Subband Phase-Shift Transform

In general, the received light $E(t)$ is equal to the sum of $E_1(t)$ and $E_2(t)$. Here, $E_1(t)$ and $E_2(t)$ are the RBS light produced by two consecutive series of reflectors, as shown in Fig. 1. The RBS light is converted into a complex signal after optical-to-electrical conversion and given by [20]

$$I(t) = I_1(t) + I_2(t) \tag{1}$$

where, $I_1(t)$ and $I_2(t)$ are the complex domain of $E_1(t)$ and $E_2(t)$. Assuming that$I(t) = A(t)\exp(j\varphi(t))$, $I_1(t) = A(t)\exp(j\varphi_1(t))$, $I_2(t) = A(t)\exp(j\varphi_2(t))$, the (1) can be expressed as

$$A(t)\exp(j\varphi(t)) = A_1(t)\exp(j\varphi_1(t)) + A_2(t)\exp(j\varphi_2(t)) \tag{2}$$

where,

$$A(t) = \sqrt{A_1(t)^2 + A_2(t)^2 + 2A_1(t)A_2(t)\cos(\varphi_1(t) - \varphi_2(t))} \tag{3}$$

Since the decomposition of the signals is difficult to implement in the time domain, the RBS light can also be described in frequency domain after Fourier transform as

$$I(\omega) = I_1(\omega) + I_2(\omega) \tag{4}$$

where, $I(\omega)$ is the frequency-domain expression of $I(t).I_1(\omega)$ and $I_2(\omega)$ are the corresponding extracted spectrums, which are expressed in frequency domain.

If the frequency component $I_2(\omega)$ is multiplied by a factor of -1, followed by an inverse Fourier transform, the signal in the time domain can be described as

$$\begin{aligned} I(t)' &= I_1(t) - I_2(t) \\ &= A_1(t)\exp(j\varphi_1(t)) - A_2(t)\exp(j\varphi_2(t)) \\ &= A_1(t)(\cos(\phi_1(t)) + j\sin(\phi_1(t))) \\ &\quad - A_2(t)(\cos(\phi_2(t)) + j\sin(\phi_2(t))) \\ &= A_1(t)\cos(\phi_1(t)) - A_2(t)\cos(\phi_2(t)) \\ &\quad + j(A_1(t)\sin(\phi_1(t)) - A_2(t)\sin(\phi_2(t))) \end{aligned} \tag{5}$$

The power of (5) can then be expressed as

$$\begin{aligned} |I(t)'|^2 &= A_1(t)\cos(\phi_1(t)) - A_2(t)\cos(\phi_2(t))^2 \\ &\quad + (A_1(t)\sin(\phi_1(t)) - A_2(t)\sin(\phi_2(t)))^2 \\ &= A_1^2(t) + A_2^2(t) \\ &\quad - 2A_1(t)A_2(t)\cos(\cos(\phi_1(t) - \phi_2(t))) \end{aligned} \tag{6}$$

Similarly, the power of (1) can be obtained based on (3) as

$$\begin{aligned} |I(t)|^2 &= A_1^2(t) + A_2^2(t) \\ &\quad + 2A_1(t)A_2(t)\cos(\cos(\phi_1(t) - \phi_2(t))) \end{aligned} \tag{7}$$

Adding (6) and (7), the combined signal power can be expressed as

$$|I(t)|^2 + |I(t)'|^2 = 2 \times (A_1^2(t) + A_2^2(t)) \tag{8}$$

From (8), it can be seen that the power of the signal after subband phase-shift transform is complementary to the power of the original signal. This characteristic can be used to mitigate the interference power fading.

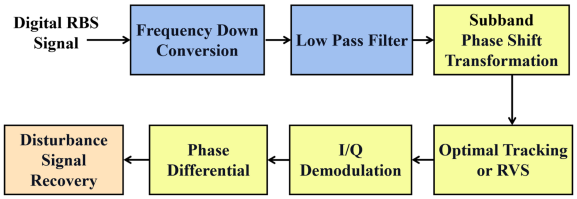

Fig. 2. Digital signal processing flow chart to mitigate the interference fading with subband phase-shift transform in Φ-OTDR.

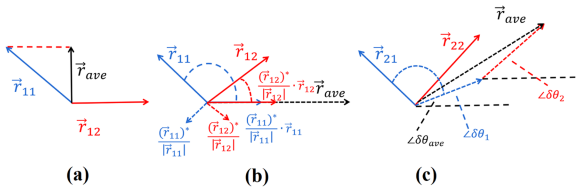

Fig. 3. (a) Direct addition of two complex RBS signal; (b) RVS method without phase noise; (c) RVS method with phase noise.

B. Demodulation Process and Methods

The data processing flow for mitigating the interference fading by subband phase-shift transform is described in Fig. 2. The subband phase-shift transform is implemented after basic pre-processing steps of frequency down conversion and low-pass filtering. As for the signal synthesis process, both optimal tracking [18] and RVS methods are investigated after subband phase-shift transform [15], [20], [21]. Finally, the characteristic of the disturbance signal can be identified after I/Q demodulation and phase differential operations.

The principle of the RVS method is shown in Fig. 3. The filtered RBS signals are represented as complex vectors. If the amplitude of the complex number is small, the interference fading may occur. When adding two complex numbers with a large difference in amplitude, the resulting vector sum is mainly determined by the complex number with the larger amplitude, and the influence of the complex number with the smaller amplitude is disregarded. On the other hand, if there is a large phase difference, the amplitude of the sum of the two complex numbers will decrease, resulting in the severe interference fading, as shown in Fig. 3(a). In Fig. 3(a), $\vec{r}_{11}$ and $\vec{r}_{12}$ are the original signal and the signal after subband phase-shift transform at the same position. It can be seen that if $\vec{r}_{11}$ and $\vec{r}_{12}$ are added directly, the amplitude may become smaller due to the large phase difference.

To eliminate the influence of the phase difference, we can use the normalized conjugate of the RBS signal obtained from the first detection $\vec{r}_{11}$ and $\vec{r}_{12}$ as references, as described in Fig. 3(b). The effect of the phase difference can be eliminated by multiplying $\vec{r}_{11}$ with $\frac{(\vec{r}_{11})^*}{|\vec{r}_{11}|}$, and the same operation for $\vec{r}_{12}$. After combining $\vec{r}_{11} \cdot \frac{(\vec{r}_{11})^*}{|\vec{r}_{11}|}$ and $\vec{r}_{12} \cdot \frac{(\vec{r}_{12})^*}{|\vec{r}_{12}|}$, $\vec{r}_{ave}$ can be obtained with enhanced amplitude. In the practical implementation of the RVS method, the subsequent RBS signal at the same position should take $\vec{r}_{11}$ and $\vec{r}_{12}$ as referrences considering the effect of noise. A simple example is illustrated in Fig. 3(c). $\vec{r}_{21}$ is a RBS signal at the same position as $\vec{r}_{11}$ in different time. In the operation of RVS, $\vec{r}_{21}$ rotates with $\vec{r}_{11}$ as a reference to eliminate the phase difference while retaining the phase induced by the disturbance signal. In the presence of noise, the phase noise $\delta\theta_1$ and $\delta\theta_2$ determines the value of residual fading noise $\delta\theta_{ave}$[15].

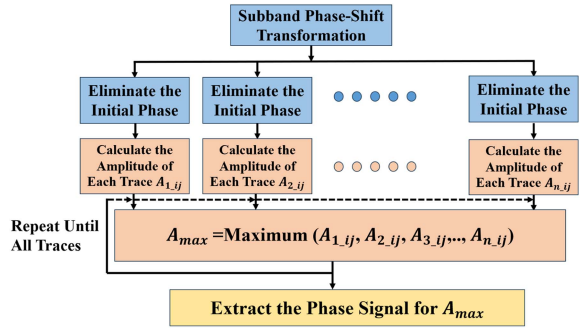

Fig. 4. Schematic diagram of the optimal tracking method.

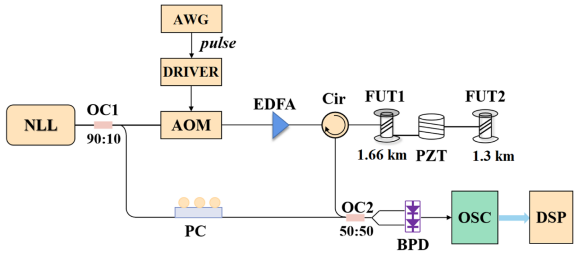

Fig. 5. Experimental setup of coherent Φ-OTDR system. NLL: narrow linewidth laser; OC: optical coupler; PC: polarization controller; AOM: acoustic optical modulator; AWG: arbitrary waveform generators; EDFA: erbium doped fiber amplifier; Cir: optical circulator; FUT: fiber under test; PZT: piezoelectric transducer; BPD: balanced photodetector; OSC: oscilloscope.

The principle of optimal tracking is also illustrated in Fig. 4. This method selects the phase with a higher SNR position by comparing the amplitudes after subband phase-shift transform. The schematic diagram of this step is shown in Fig. 4 [18]. After subband phase-shift transform, the initial phase of the signal with different phase-shift transform is different. Because the phase change is continuous, the initial phase will be accumulated after continuous change. After elimination of the initial phase, the phase of all signals is at the same level, and there is no jump during the phase selection process. Then, the amplitude of each point in each trace is calculated. By comparing these amplitudes, the corresponding point with high SNR can be found, so as to avoid the fading points. These steps are repeated for each trace to demodulate the correct phase. After phase selection using the optimal tracking method, the phases of all points are characterized by a relatively high SNR. In the subsequent analysis, we will compare the demodulation results obtained through the RVS and optimal tracking methods.

III. Experimental Setup

The experimental setup is illustrated in Fig. 5. A laser with a linewidth of 3 kHz is used as the light source. The laser beam is split into two parts using a 90:10 coupler, where 10% of the light is used as the local oscillator, while the remaining 90% is

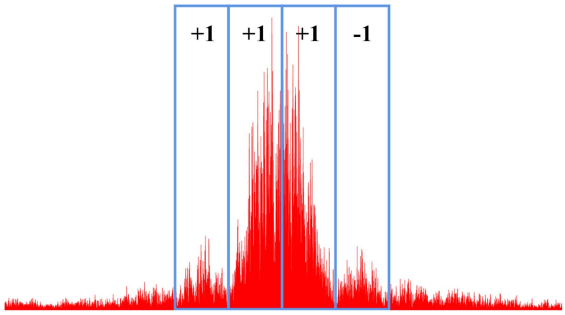

Fig. 6. Illustration of the signals extraction in frequency domain.

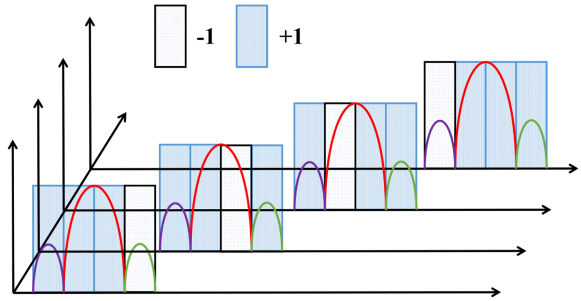

Fig. 7. Four-time phase-shift transform and the illustration of the signal extraction.

used for optical pulse generation. In the experiment, an electrical rectangular pulse with a width of 100 ns and a frequency of 25 kHz is generated by an arbitrary waveform generator (AWG) as the probe signal. The output signal of AWG is then amplified to 3.3 V to drive the AOM. This electrical signal is then converted to an optical signal through an acousto-optic modulator (AOM). Then the optical signal is transmitted through a fiber after passing through an erbium-doped fiber amplifier (EDFA). The RBS light is sent back to the local oscillator via an optical circulator and combined at a 2×2 coupler. The resulting RBS signal is detected using a balanced photodetector (BPD) and collected by an oscilloscope (OSC) operating at a sampling rate of 500 MSa/s. The disturbance signal is generated by a function generator with adjustable amplitude and frequency, and then added through a piezoelectric transducer (PZT) located at 1.6 km of the fiber link. The length of FUT1 is $\sim$1.6 km, and the length of FUT2 is $\sim$1.3 km.

IV. Experimental Results and Discussions

Based on the principle described in section II-A, the signals with complementary amplitude can be obtained after subband phase-shift transform. Therefore, the subband of the RBS signal should be first extracted, as shown in Fig. 6. In order to mitigate the effect of out-of-band noise, only the main band and the first order sideband are considered. Then one subband is chosen to implement the phase-shift operation by multiplying a factor of -1.

In order to effectively mitigate the interference fading points, several phase-shift transforms can be implemented with different subband bandwidth at the cost of multiple subband extraction operations with high computational complexity [20]. To reduce the computational complexity, the phase-shift operation can be implemented among the subbands with the same bandwidth, as shown in Fig. 7. Each subband is extracted and then multiplied by a factor of -1. Therefore, four-time phase-shift transform are implemented in our work with only one-time subband extraction operation.

The complementary characteristic of signal after phase-shift transform are illustrated in Fig. 8, where two-time subband phase-shift transform is taken as an example at different positions. It can be seen that when the amplitude of the original is low, the amplitude of the transformed signal in blue line tends to be relatively high, as shown in Fig. 8(a). In Fig. 8(b), however, when

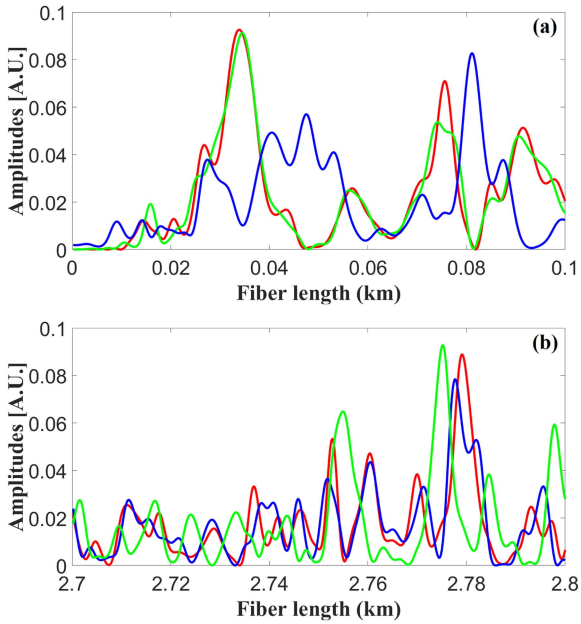

Fig. 8. Amplitudes of original signal and signal after two-time phase-shift transform at (a) distance between 0 to 0.1 km and (b) distance between 2.7 to 2.8 km.

both the signal in red line and blue line are at a relatively low level, the amplitude of the transformed signal in green line tends to be relatively high, verifying the complementary characteristic of subband phase-shift transform.

The intensity fluctuations of the signal with and without subband phase-shift transform are shown in Fig. 9. From Fig. 9(a), it can be seen that the original signal has a large intensity fluctuation of $\sim$70 dB. With one-time subband phase-shift transform, the intensity fluctuation is reduced to be $\sim$50 dB, as shown in Fig. 9(b). In Fig. 9(c), the intensity fluctuation is further reduced to $\sim$32 dB after two-time subband phase-shift transform. The intensity fluctuation can be reduced to as low as $\sim$20 dB with four-time subband phase-shift transform, as shown in Fig. 9(d).

Next, the phase differential result is presented in Fig. 10. From Fig. 10(a), it can be seen that the phase of the original signal has many falses due to the interference fading. As shown in Fig. 10(b) and (c), most of the false phases can be suppressed

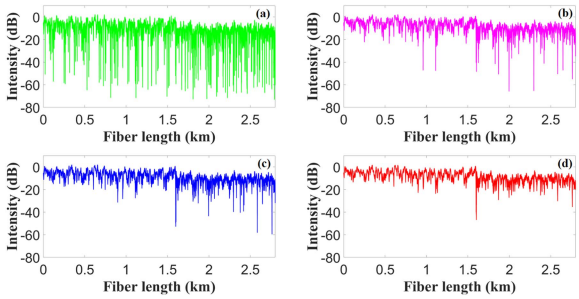

Fig. 9. (a) Intensity fluctuation of the original signal; (b) the intensity fluctuations of the signal after one-time subband phase shift transform; (c) the intensity fluctuations of the signal after two-time subband phase shift transform; (d) the intensity fluctuations of the signal after four-time subband phase shift transform.

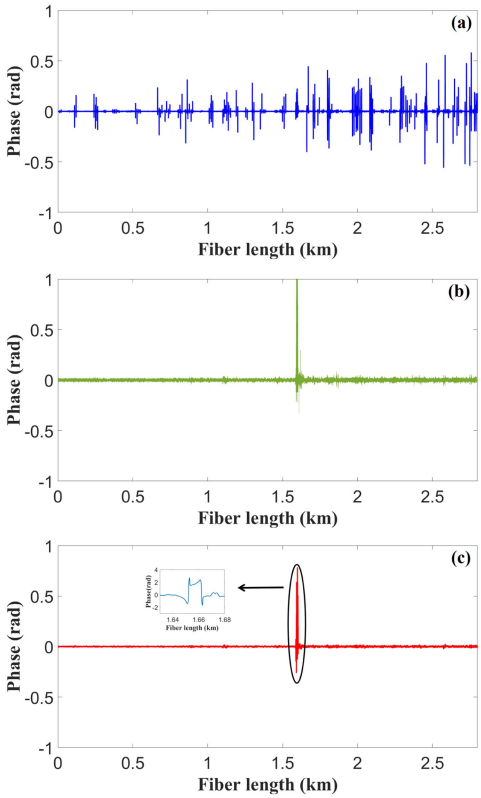

Fig. 10. Normalized phase differential demodulation results with (a) original signal, (b) optimal tracking method, and (c) RVS method.

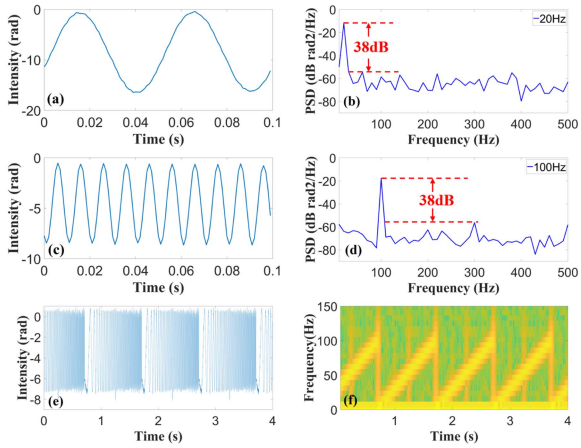

Fig. 11. Characterization of the disturbance signal. (a) Measured time-domain signal and (b) the corresponding frequency spectrum of the 20 Hz vibration; (c) measured time-domain signal and (d) the corresponding frequency spectrum of the 100 Hz vibration; (e) measured time-domain signal and (f) the corresponding frequency spectrum of the frequency-chirped vibration.

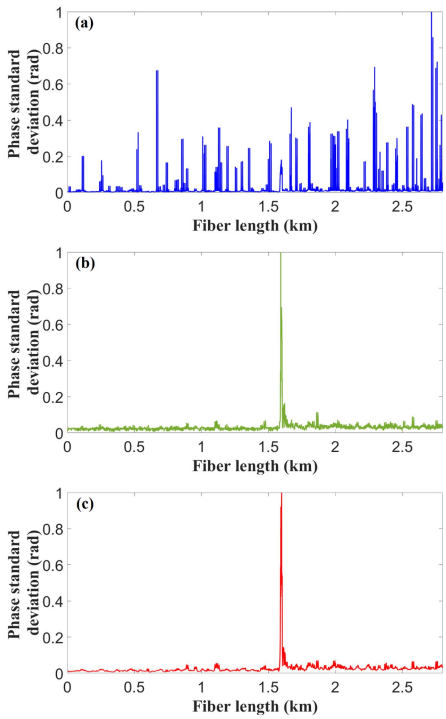

Fig. 12. Comparison of the phase standard deviation after different processing methods. (a) The phase standard deviation of the original signal. (b) The phase standard deviation of the signal with four-time phase-shift transform and optimal tracking. (c) The phase standard deviation of the signal with four-time phase-shift transform and RVS.

after subband phase-shift transform, followed by optimal tracking and RVS methods.

Then, we conduct dynamic measurements to study the recovery performance of the disturbances signal. In the experiment, we applied two sinusoidal waveforms to the fiber with frequencies of 20 Hz and 100 Hz. The time-domain waveforms of these vibrations are presented in Fig. 11(a) and (c), respectively. The corresponding power spectral densities (PSDs) are also calculated in Fig. 11(b) and (d). It is shown that the disturbance signal is successfully recovered with an SNR of ∼38 dB. Furthermore, a chirp waveform within the 0–100 Hz frequency range was also tested. The corresponding time-domain signal can be observed in Fig. 11(e). To analyze the frequency spectrum, the short-time Fourier transform is employed, and the result is displayed in Fig. 11(f).

We also use the standard deviation of the differential phase to evaluate the effectiveness of the interference fading mitigation [22]. As shown in Fig. 12(a), it can be seen that the interference fading of the original signal along the fiber is strong,

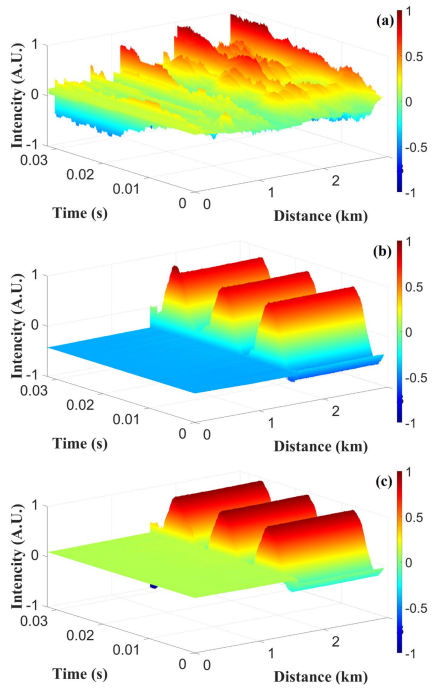

Fig. 13. Temporal-spatial images of the demodulated phase value with (a) original signal, (b) signal with four-time phase-shift transform and optimal tracking, and (c) signal with four-time phase-shift transform and RVS.

and the standard deviation at some points are even larger than the intensity of the vibration. The calculated average phase standard deviation is as large as 0.223 rad. It is also shown in Fig. 12(b) and (c) that the phase standard deviation is reduced to be 0.105 rad and 0.046 rad by optimal tracking and RVS methods after four-time subband phase-shift transform, respectively. The lower phase standard deviation indicates that subband phase-shift transform can achieve lower phase noise with high measurement accuracy. The effectiveness of the proposed method is also verified via the temporal-spatial images of the demodulated phase in Fig. 13. It is shown in Fig. 13(a) that the color changes occur irregularly at many random positions due to the interference fading. After four-time phase-shift transform, the phase change at the disturbance zone is more prominent, which indicates that both optimal tracking and RVS method can effectively suppress the interference fading, as shown in Fig. 13(b) and (c).

V. Conclusion

This paper examines the causes of interference fading in coherent Φ-OTDR and proposes an efficient method for mitigating the interference fading. The proposed method is based on subband phase-shift transform and combines two different techniques. By appropriately decomposing the detected signal and applying subband phase shifts to different components, signals with the complementary amplitudes can be obtained. These amplitude complementary signals can then be synthesized to correct false phases induced by the interference fading. It is noted that this method does not require complex frequency modulation, and it can effectively recover the vibration waveform. The proposed method contribute a new insight into the mitigation of the interference fading and improving the coherent Φ-OTDR performance.

References

[1] X. Bao, D. J. Webb, and D. A. Jackson, "32-KM distributed temperature sensor based on Brillouin loss in an optical fiber," *Opt. Lett.*, vol. 18, no. 18, pp. 1561–1563, 1993.
[2] Y. Chen, Q. Han, T. Liu, X. Lan, and H. Xiao, "Optical fiber magnetic field sensor based on single-mode–multimode–single-mode structure and magnetic fluid," *Opt. Lett.*, vol. 38, no. 20, pp. 3999–4001, 2013.
[3] X. He et al., "Multi-event waveform-retrieved distributed optical fiber acoustic sensor using dual-pulse heterodyne phase-sensitive OTDR," *Opt. Lett.*, vol. 42, no. 3, pp. 442–445, 2017.
[4] P. Jousset et al., "Dynamic strain determination using fibre-optic cables allows imaging of seismological and structural features," *Nature Commun.*, vol. 9, no. 1, 2018, Art. no. 2509.
[5] J. Tejedor et al., "Toward prevention of pipeline integrity threats using a smart fiber-optic surveillance system," *J. Lightw. Technol.*, vol. 34, no. 19, pp. 4445–4453, Oct. 2016.
[6] J. C. Juarez and H. F. Taylor, "Field test of a distributed fiber-optic intrusion sensor system for long perimeters," *Appl. Opt.*, vol. 46, no. 11, pp. 1968–1971, 2007.
[7] Z. Zhao et al., "Interference fading suppression in Φ-OTDR using space-division multiplexed probes," *Opt. Exp.*, vol. 29, no. 10, pp. 15452–15462, 2021.
[8] Z. Zhao et al., "Enabling simultaneous DAS and DTS through space-division multiplexing based on multicore fiber," *J. Lightw. Technol.*, vol. 36, no. 24, pp. 5707–5713, Dec. 2018.
[9] Z. Zhao, M. Tang, L. Wang, N. Guo, H.-Y. Tam, and C. Lu, "Distributed vibration sensor based on space-division multiplexed reflectometer and interferometer in multicore fiber," *J. Lightw. Technol.*, vol. 36, no. 24, pp. 5764–5772, Dec. 2018.
[10] Z.-W. Ding et al., "Phi-OTDR based on-line monitoring of overhead power transmission line," *J. Lightw. Technol.*, vol. 39, no. 15, pp. 5163–5169, Aug. 2021.
[11] Z. Wang et al., "Coherent Φ-OTDR based on I/Q demodulation and homodyne detection," *Opt. Exp.*, vol. 24, no. 2, pp. 853–858, 2016.
[12] G. Tu, X. Zhang, Y. Zhang, F. Zhu, L. Xia, and B. Nakarmi, "The development of an Φ-OTDR system for quantitative vibration measurement," *IEEE Photon. Technol. Lett.*, vol. 27, no. 12, pp. 1349–1352, Jun. 2015.
[13] X. Fan, G. Yang, S. Wang, Q. Liu, and Z. He, "Distributed fiber-optic vibration sensing based on phase extraction from optical reflectometry," *J. Lightw. Technol.*, vol. 35, no. 16, pp. 3281–3288, Aug. 2017.
[14] H. He, L. Yan, H. Qian, X. Zhang, B. Luo, and W. Pan, "Enhanced range of the dynamic strain measurement in phase-sensitive OTDR with tunable sensitivity," *Opt. Exp.*, vol. 28, no. 1, pp. 226–237, 2020.
[15] D. Chen, Q. Liu, and Z. He, "Phase-detection distributed fiber-optic vibration sensor without fading-noise based on time-gated digital OFDR," *Opt. Exp.*, vol. 25, no. 7, pp. 8315–8325, 2017.
[16] Y. Wu, Z. Wang, J. Xiong, J. Jiang, S. Lin, and Y. Chen, "Interference fading elimination with single rectangular pulse in Φ-OTDR," *J. Lightw. Technol.*, vol. 37, no. 13, pp. 3381–3387, Jul. 2019.
[17] K. Cui et al., "Interference-fading-suppressed pulse-coding Φ-OTDR using spectrum extraction and rotated-vector-sum method," *IEEE Photon. J.*, vol. 13, no. 6, Dec. 2021, Art. no. 6800206.
[18] M. Zabihi et al., "Continuous fading suppression method for Φ-OTDR systems using optimum tracking over multiple probe frequencies," *J. Lightw. Technol.*, vol. 37, no. 14, pp. 3602–3610, Jul. 2019.
[19] J. Xiong, Z. Wang, Y. Wu, H. Wu, and Y. Rao, "Long-distance distributed acoustic sensing utilizing negative frequency band," *Opt. Exp.*, vol. 28, no. 24, pp. 35844–35856, 2020.
[20] H. He et al., "Suppression of the interference fading in phase-sensitive OTDR with phase-shift transform," *J. Lightw. Technol.*, vol. 39, no. 1, pp. 295–302, Jan. 2021.
[21] H. Qian et al., "Fading-free Φ-OTDR with multi-frequency decomposition," *IEEE Sensors J.*, vol. 22, no. 3, pp. 2160–2166, Feb. 2022.
[22] D. Chen, Q. Liu, and Z. He, "High-fidelity distributed fiber-optic acoustic sensor with fading noise suppressed and sub-meter spatial resolution," *Opt. Exp.*, vol. 26, no. 13, pp. 16138–16146, 2018.